Journal of Applied Polymer Science

Development of Magnetic Fabrics with Tunable Hydrophobicity

Thu Ho, Negar Ghochaghi, Gary Tepper
Department of Mechanical and Nuclear Engineering, Virginia Commonwealth University, Richmond, Virginia 23284
Correspondence to: G. Tepper (E-mail: gctepper@vcu.edu).

ABSTRACT: Polystyrene (PS) fiber mats incorporating iron (Fe) particles were fabricated by electrospinning and the hydrophobicity of the resulting magnetic fabrics was investigated with and without an applied magnetic field. The results show that the hydrophobicity increases in the presence of a magnetic field and the hysteresis in the advancing/receding contact angle decreases in the presence of a magnetic field. It is also shown that the contact angle and hysteresis increase with decreasing fiber diameter. © 2013 Wiley Periodicals, Inc. J. Appl. Polym. Sci. 130: 2352–2358, 2013

KEYWORDS: electrospinning; fibers; polystyrene

Received 10 June 2012; accepted 6 February 2013; Published online 25 May 2013
DOI: 10.1002/app.39340

INTRODUCTION

Superhydrophobic surfaces are characterized by a water droplet contact angle (WCA) larger than 150° and are being investigated for applications including self-cleaning surfaces and drag reduction.[1] Superhydrophobic surfaces arise in nature (e.g., the Lotus leaf) and are the result of a combination of hydrophobicity (low surface free energy) and micro or nanoscale surface roughness.[2] Synthetic superhydrophobic surfaces have been produced using many techniques including layer-by-layer deposition,[3] chemical deposition,[4] sol–gel processing[5] solution casting,[6] laser/plaster/chemical etching,[7] lithography,[8] and electrospinning.[9,10] In recent years, electrospinning has attracted significant attention for its ability to produce polymer or polymer composite fibrous mats with high specific surface area and micro or nanoscale surface roughness.[11–14] In this article electrospinning was used to produce hydrophobic and superhydrophobic polystyrene and polystyrene/iron composite fibrous mats with different average fiber diameter and mat thickness. Contact angle measurements were performed to determine the effect of surface morphology and magnetic environment on hydrophobicity. The purpose of this initial article is to present our preliminary qualitative findings on the hydrophobicity of polystyrene/Fe magnetic fabrics. The ability to adjust the hydrophobicity of a surface or fabric using an externally applied magnetic field could have many applications in areas such as liquid sampling, microfluidics, flow control, and surface chemistry.

EXPERIMENTAL

Material

Polystyrene (PS) with average molecular weight of ~350,000, toluene and dimethylformamide (DMF) were purchased from Sigma–Aldrich, and used as received without further purification. Iron nanopowders (60–80 nm) were purchased from READE Advanced Materials.

Preparation of Polymer Solutions

PS solutions were prepared at four different concentrations ranging from 10 to 25% by weight. The solvent composition was kept constant at 70% toluene and 30% DMF. PS concentrations, however, were varied to achieve various fiber diameters. PS as purchased came as solid beads. Therefore, after being added to the solvent at a designated weight percent, the solution was left to dissolve for an extended amount of time (typically 24 h) to ensure homogeneous solvation. Magnetic fabrics were produced by adding iron nanoparticles (60–80 nm) to the prepared PS solutions at the same weight percent as the PS beads. Therefore, after solvent evaporation, the resulting dry fabric consists of half PS and half Iron particles by weight. Iron nanoparticles as purchased are pyrophoric, which means they can ignite spontaneously in air. Therefore, the process of adding these particles to the PS solutions was performed inside of a glove box filled with inert gas (Argon). The nanoparticles also tend to agglomerate. Therefore, after the solutions were prepared; they were sonicated for several hours before electrospinning. Branson 2510 Ultrasonic Cleaner was used as an ultrasonic bath for this purpose. The magnetic PS solutions were electrospun shortly after the sonication.

Electrospinning of PS and PS/Fe Composite Coatings

Electrospinning is a process that employs electrostatic forces to draw polymer fibers from a solution. The main components of the electrospinning process are shown in Figure 1 and consist of a syringe feeder system containing the polymer solution, a collector system where the fiber will be deposited and a high

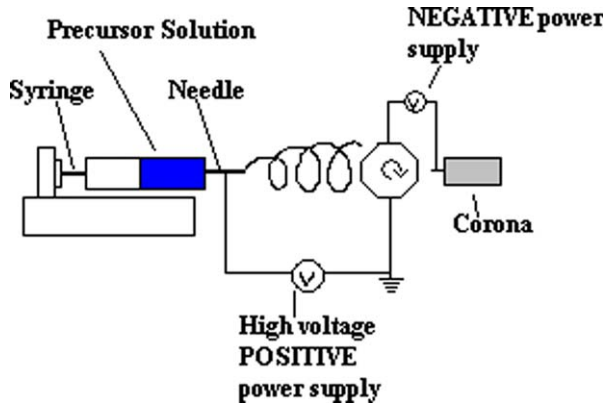

Figure 1. Schematic diagram of electrospinning components. [Color figure can be viewed in the online issue, which is available at wileyonlinelibrary.com.]

voltage power supply to provide the electrical force. However, because the fibers are electrically charged, surface deposition can be impeded by surface charge accumulation, particularly on surfaces with very low electrical conductivity. Deposition can even be impeded on conducting substrates if the deposited polymer layer becomes sufficiently thick to electrically insulate the surface, thereby preventing charge dissipation. In this case, the positively charged substrate repels the positively charged fibers and prevents deposition. Previously we showed that a negative ion source, used in conjunction with a positively charged electrospinning source, can be used to neutralize surface charges *in situ* and facilitate uniform fiber deposition.[15] The fiber diameter in an electrospinning process can be adjusted by changing processing parameters such as solute concentration, solution conductivity, electrostatic force and liquid surface tension. For the polystyrene solutions used in this study, the polystyrene fiber diameters were adjusted by changing the solute concentration while keeping other parameters constant. The flow rate was set to 0.8 μL min^{-1}. The distance between the needle tip and the drum axis was 7 cm. The corona was placed 4.5 mm from drum surface, its tip coaxial to the needle tip. A negative voltage of 3.5 kV was given to the corona. DC positive voltage was varied for different solutions to achieve a stable jet and was recorded in Table I. The electrospinning time was also varied depending on the objective of the experiment.

To study the effect of fiber diameter, electrospun PS mats were deposited onto glass substrates from 10, 15, 20, and 25% solutions by weight for 10, 6.7, 5, and 4 min, respectively. The deposition times were reduced with increasing polymer concentration to produce fiber coatings of equivalent mass.

Fiber mats of increasing weight/thickness were also deposited from 25% PS solutions on a glass substrate to investigate the effect of the mat thickness on hydrophobicity and hysteresis. The coating weight/thickness was varied by increasing the deposition time from 2 to 5 min with all other processing parameters remaining constant.

To study the effect of embedded Iron nonoparticles inside PS fiber mats, PS solutions at two different concentrations (10 and 25%) were mixed with the same weight of iron nanoparticles. The mixtures were then sonicated for several hours to ensure the separation of particles. The sonicated PS solutions of 10 and 25% were then electrospun onto glass substrates for 10 and 5 min, respectively to produce PS–iron composite fiber mats.

Characterization

Surface Morphology. The average fiber diameter and the overall surface morphology of the mats were determined by the method of scanning electron microscopy.

Hydrophobicity and Hysteresis. The water contact angle and hysteresis (difference in advancing and receding contact angles) were measured with a Game-hart Model 500 Advanced Goniometer. For the measurement of contact angles, droplet size was kept constant at a volume of about 5 μL (2.1-mm droplet diameter). Two different types of permanent magnets (rare earth ring magnet and horseshoe) were used to test the effect of a magnetic field on the hydrophobicity of the magnetic-particle-embedded mats. The horseshoe magnet is a regular lab magnet and, therefore, does not exhibit strong magnetic field. The ring magnet is a very strong Grade N42 Neodymium rare earth magnet with Br_{max} of 13200 Gauss and BH_{max} of 42 MGOe.

Thermal Gravimetric Analysis (TGA). Because the vast majority of the magnetic particles were embedded within the PS fibers, scanning electron microscopy (SEM) could not be used to visualize the particle distribution within the fibers. Therefore, TGA was used to ensure that the fiber mats contain the same weight composition of PS and Iron nanoparticles (1 : 1) after electrospinning. Preweighed samples were heated in the TGA furnace to remove the PS and then weighed again to determine the weight of the remaining iron particles. After PS removal, the mats were imaged again using scanning electron microscopy to determine the uniformity of the particle distribution.

RESULTS AND DISCUSSION

Effect of Mat Fiber Diameter

Figure 2(a–d) show SEM images of the resulting fiber mats electrospun from 10, 15, 20, and 25% PS solutions and Table II gives the average fiber diameter for each PS concentration. From the images in Figure 2 it can be seen that, in addition to a decrease in fiber diameter with decreasing PS concentration, there is also a change in morphology. At PS concentrations below 20% large beads begin to form along the length of the fibers. The beads are evident in Figure 2(b) (15% solution) and

Table I. DC Voltage Parameter for Different PS Solutions

Solution	10% PS	15% PS	20% PS	25% PS	10% PS with iron particles	25% PS with iron particles
DC voltage (kV)	7	7.3	8.5	9	8	9

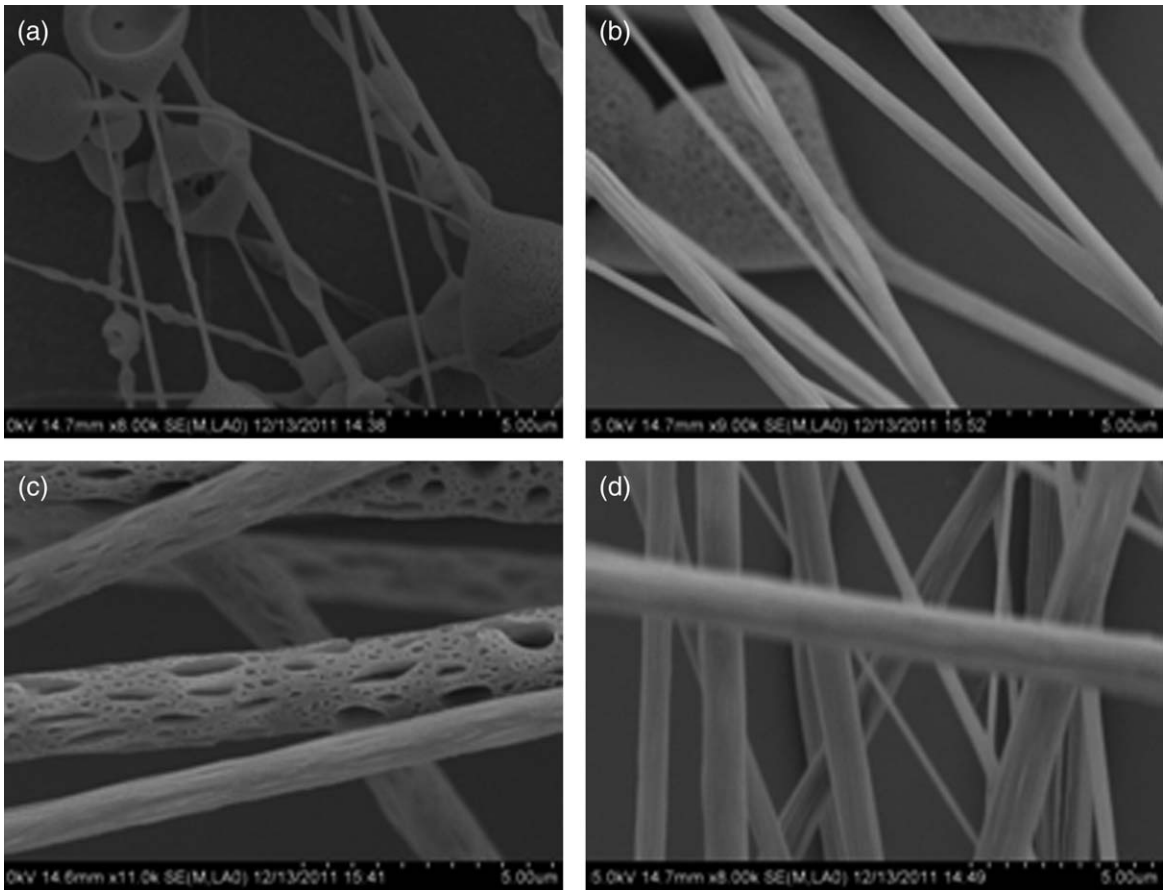

Figure 2. a. SEM image of fibers electrospun from 10% PS solution. b. SEM image of fibers electrospun from 15% PS solution. c. SEM image of fibers electrospun from 20% PS solution. d. SEM image of fibers electrospun from 25% PS solution.

become profuse in Figure 2(a) (10% solution). The so called "bead-on-string" morphology is very common in electrospinning.[16–18] The presence of the beads in the lower concentration samples makes it difficult to directly correlate the measured hydrophobicity with changes in fiber diameter alone since another morphological change (the formation of beads) is also occurring. The average fiber diameters reported here were obtained from the fiber regions of the mats (between the beads).

Figures 3 and 4 show the water contact angle and hysteresis measurements of each of the samples. The data of Figure 3 shows that the contact angle decreases significantly (by $\sim$16°) as the average fiber diameter increases by 600 nm. The data of Figure 4 shows that the contact angle hysteresis decreases by nearly 40° as the average fiber diameter increases by 600 nm.

The water droplet contact angle is a measure of the wettability of a surface and if the contact angle is $<$90°, the surface is deemed hydrophilic whereas if the contact angle is $>$90°, the surface is hydrophobic. If the contact angle is between 150° and 180°, the surface is superhydrophobic. A droplet may form either a homogeneous interface on a solid surface, or a composite interface on a rough surface where air pockets trapped between the surface and the droplet form a nonwetting phase and this composite interface is what leads to the very large contact angles characteristic of superhydrophobicity. The fiber-based surfaces prepared and characterized in this article result in a composite interface where the fibers form the wetting phase and the spaces between the fibers are filled with air and form the nonwetting phase. The Wenzel equation developed for a homogeneous solid-liquid interface was extended by Cassie and Baxter for the composite interface.[19–21] The contact angle for the composite surface can be calculated with the following equation

$$\cos\theta = R_f f_{SL} \cos\theta_o - f_{LA} \quad (1)$$

where θ is the contact angle of the rough surface, θ_o is the contact angle of the smooth surface, R_f is the roughness factor,

Table II. Average Fiber Diameter for Electrospun Mats of Different PS Concentration

	10%	15%	20%	25%
Diameter (μm)	0.22 ± 0.08	0.5 ± 0.11	1.13 ± 0.25	1.23 ± 0.27

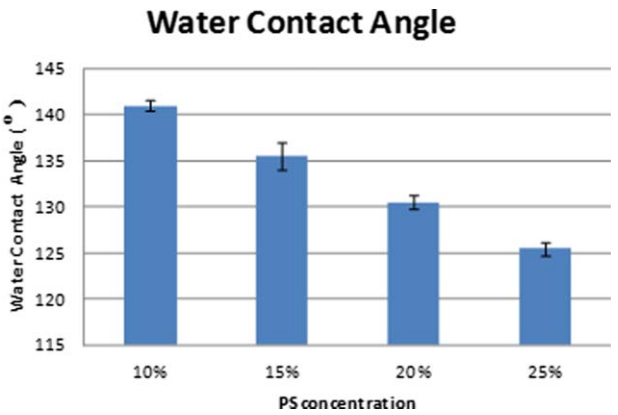

Figure 3. Effect of fiber diameter—water contact angle. [Color figure can be viewed in the online issue, which is available at wileyonlinelibrary.com.]

defined as the ratio of the solid–liquid area to its projection on a flat lane, f_{SL} and f_{LA} are fractional geometrical areas of the solid–liquid and liquid–air interfaces under the droplet, respectively. From this equation, it can be seen that the contact angle on the rough surface depends on both geometric factors as well as the contact angle of the smooth surface (a measure of the surface free energy).

The increase in contact angle with decreasing average fiber diameter indicates that the surface roughness factor (the fractional percentage of the water droplet contacting the wetting phase (polymer) versus the nonwetting phase (air)) is higher for the mats with fine fibers and large diameter beads. The contribution of the beads to the roughness factor is expected to be significant based on the images of Figure 2, but has not been quantified in the present study.

Contact angle hysteresis, the difference between the advancing and receding contact angles of a droplet moving along a surface, can be used to characterize the "stickiness" of a hydrophobic surface.[22] A low contact angle hysteresis suggests a very low water roll-off angle (the angle at which the droplet will roll off the surface) and this property is very important in some applications such as self-cleaning surfaces and drag reduction. A high contact angle hysteresis results in a high roll-off angle and in extreme cases can result in the so-called gecko state where a water droplet sticks to the surface and the surface can be inverted with the water droplet suspended beneath.[23] That is, while somewhat counterintuitive, a surface can be both sticky and superhydrophobic. A water droplet placed onto a sticky superhydrophobic surface will have a very high contact angle but will also adhere to the surface.

The data of Figure 4 shows that the contact angle hysteresis increases significantly with decreasing average fiber diameter. This means that the surface is becoming stickier (transition to gecko state) as the average fiber diameter decreases but this result is more difficult to explain in terms of the observed fabric morphologies. One possibility is that, because of capillarity, the gecko state is favored by the presence of a multitude of small air pockets rather than a few large air pockets.

Effect of Mat Thickness

The SEM images of PS fiber samples electrospun for increasing time period are shown in Figure 5(a–d). Figures 6 and 7 shows the water contact angle and hysteresis measurements of the 25% PS samples as a function of deposition time. The results show that increasing the mat thickness initially decreases both the water contact angle as well as the contact angle hysteresis and then levels off. We believe that this indicates that the fiber density (number of fibers per unit surface area) initially increases during the time below 4 min when the first complete fiber layer is being formed. After the creation of the first complete layer, the fiber density at the surface remains essentially constant and the observed changes in contact angle and hysteresis with deposition time are small. The incomplete fiber layer will exhibit a higher roughness factor since the ratio of the wetting phase to the nonwetting phase is small (few fibers) and will, therefore, have a higher contact angle than the thicker layers. The incomplete fiber layer will also exhibit higher capillary forces (larger hysteresis) because the air pockets formed between the fibers terminate on the glass substrate and form a closed air pocket. In thicker fiber mats containing multiple layers the air pockets are open and connected through pathways between layers and, therefore, the capillary forces are reduced along with the observed contact angle hysteresis.

Magnetic Particle Embedded in Polystyrene Fiber

Magnetic composite fibers, in which magnetic nanoparticles are embedded into a polymeric fiber matrix, have been previously fabricated and exhibit many interesting properties under the influence of a magnetic field.[24–26] Magnetic fabrics have a wide range of potential applications such as electromagnetic interference shielding, biomedical sensing and magneto-optical storage.[25] Our work explores the possibility of using magnetic fabrics to control surface superhydrophobicity and adhesion.

It should be noted that pure PS fiber mats (with no Iron particle embedded) were also tested for water contact angle and hysteresis under the influence of a magnetic field. Results of this experiment showed that the water contact angle and hysteresis properties of the pure PS fiber mats do not change under the application of a magnetic field. Therefore the embedded nanoparticles inside the magnetic fiber are assumed to be responsible for the observed change in water contact angle and hysteresis

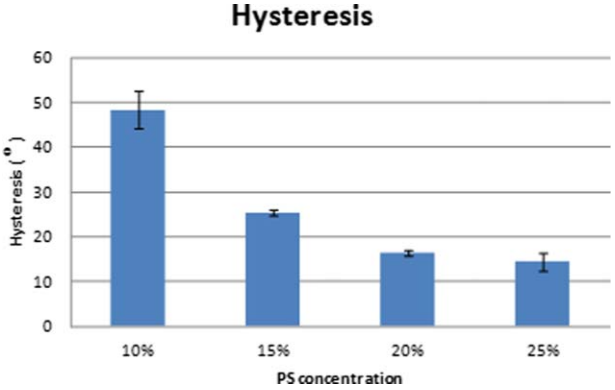

Figure 4. Effect of fiber diameter—hysteresis. [Color figure can be viewed in the online issue, which is available at wileyonlinelibrary.com.]

Applied Polymer SCIENCE

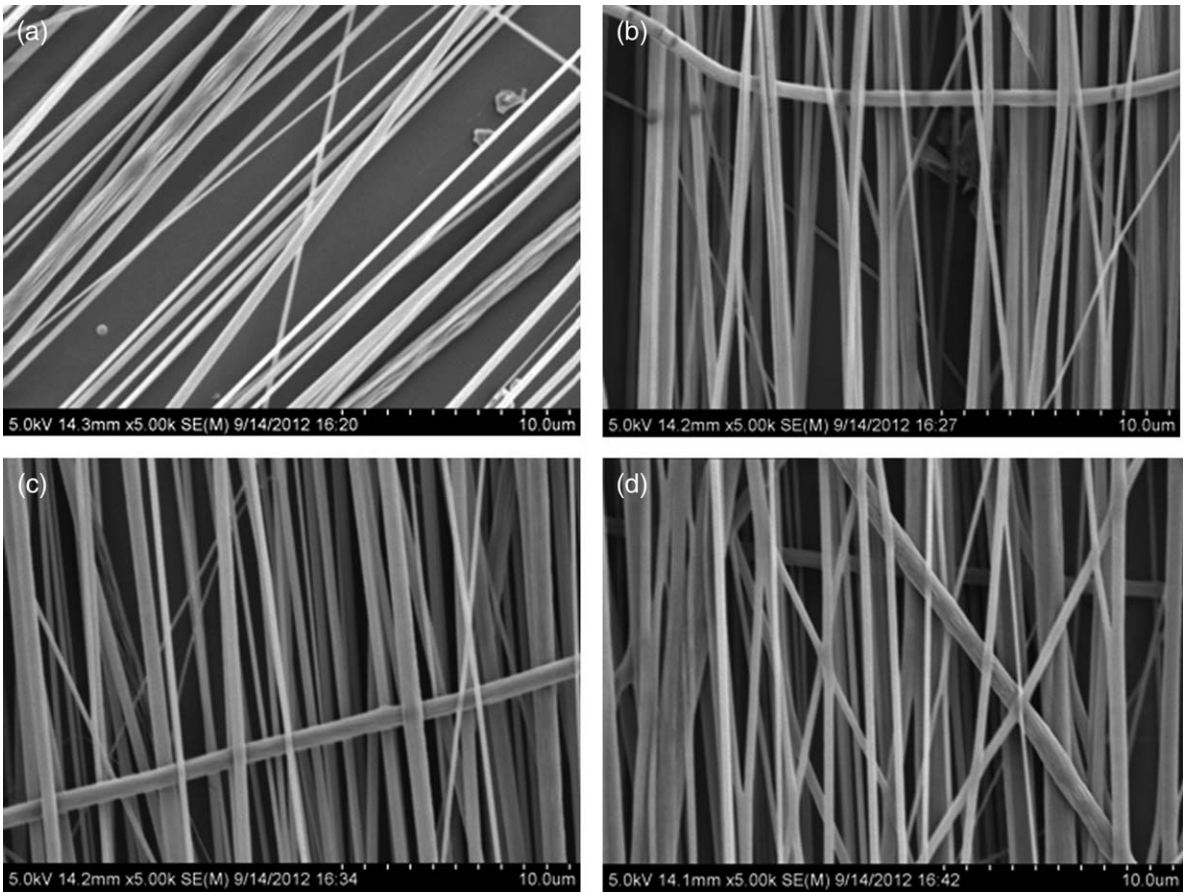

Figure 5. a: SEM image of PS fibers electrospun in 2 min. b: SEM image of PS fibers electrospun in 3 min. c: SEM image of PS fibers electrospun in 4 min. d: SEM image of PS fibers electrospun in 5 min.

properties of the magnetic fiber mats with the application of magnetic field.

The morphologies of the composite mats of PS and Iron nanoparticles were studied using SEM and are shown in Figure 8(a–c).

The majority of the magnetic particles were found to be embedded within the PS fibers and do not appear clearly in the SEM images. The magnetic particles were added at the same weight as the PS. Therefore, after solvent evaporation, the resulting mats should consist of 50% PS and 50% iron by weight. TGA was performed on the samples and the results confirm that the magnetic particles were embedded inside the PS fibers. Figure 9 shows microscope images of a composite mat before and after PS removal illustrating the relatively uniform dispersion of the iron particles within the fibers.

Figures 10 and 11 show the water contact angle and hysteresis measurements of the 10 and 25% PS/iron composite samples with and without the application of a magnetic field and for two different types of permanent magnets (rare earth bar

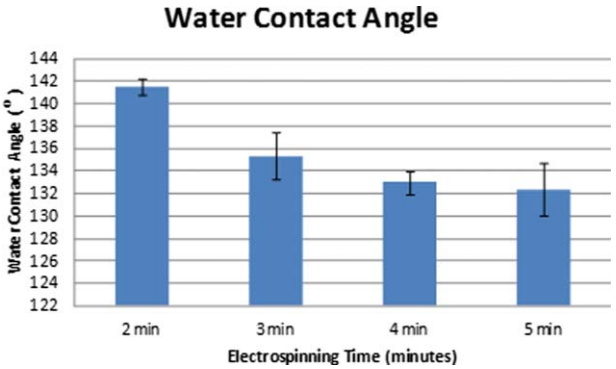

Figure 6. Effect of mat thickness—water contact angle of 25% PS mats. [Color figure can be viewed in the online issue, which is available at wileyonlinelibrary.com.]

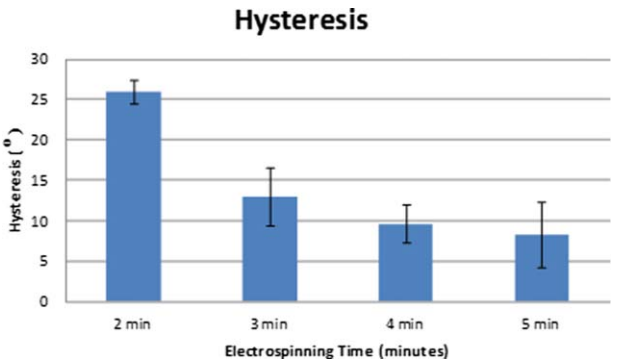

Figure 7. Effect of mat thickness—hysteresis of 25% PS mats. [Color figure can be viewed in the online issue, which is available at wileyonlinelibrary.com.]

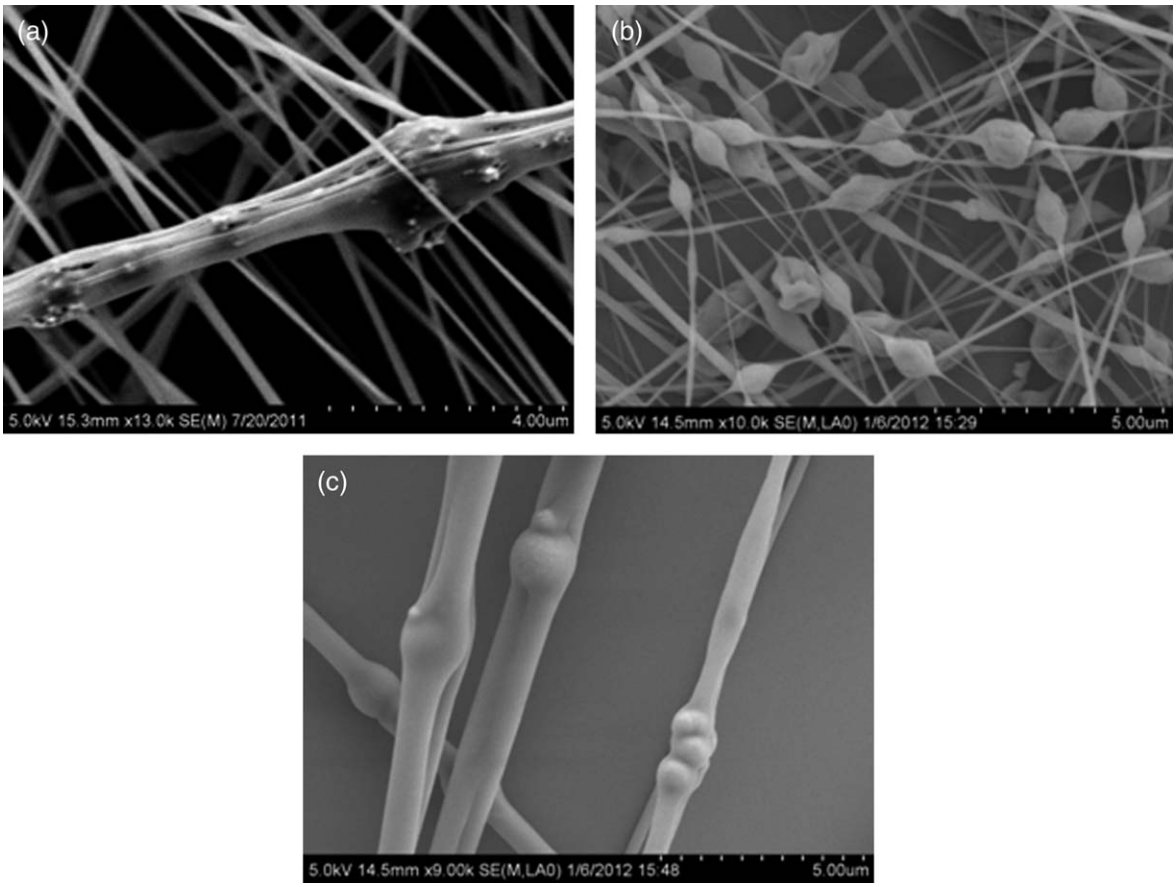

Figure 8. a: Close-up of a magnetic particle embedded fiber. b: 10% PS fiber with embedded particles. c: 25% PS fiber with embedded particles.

magnet and horseshoe). We do not have quantitative data on the relative strength of the two magnets and our contact angle apparatus made it very difficult to vary the magnet position to affect field strength and orientation. The rare earth ring magnet is Grade N42 neodymium rare earth magnet with Br_{max} of 13200 Gauss and BH_{max} of 42 MGOe and is therefore much stronger than the regular lab-use horseshoe magnet. The measurements were repeated multiple times to ensure statistically significant reproducible results and the error bars in the data were calculated from the statistics of the measurement set. The results show that the externally applied magnetic field slightly increases the water droplet contact angle for both fiber diameters and for both types of magnets. However, the increase is largest when using the rare earth magnet and 25% PS solution (larger diameter), and the water droplet contact angle increases by about 10°. The results also show that the magnetic field reduces the water droplet contact angle hysteresis by up to 10°, but only for the 10% PS fibers. We believe that since 10% PS fibers have significantly higher hysteresis than 25% PS, as previously discussed above, the effect of magnetic field on fiber hysteresis will be more pronounced.

We believe that the observed increase in water droplet contact angle in the presence of a magnetic field is due to a field-induced

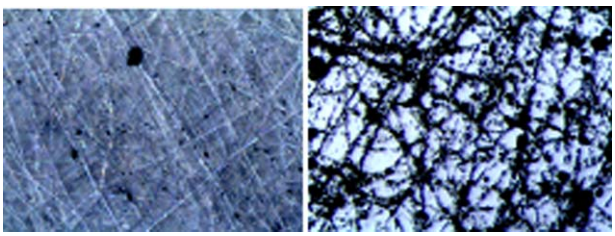

Figure 9. Microscopic image of a composite mat before and after TGA. [Color figure can be viewed in the online issue, which is available at wileyonlinelibrary.com.]

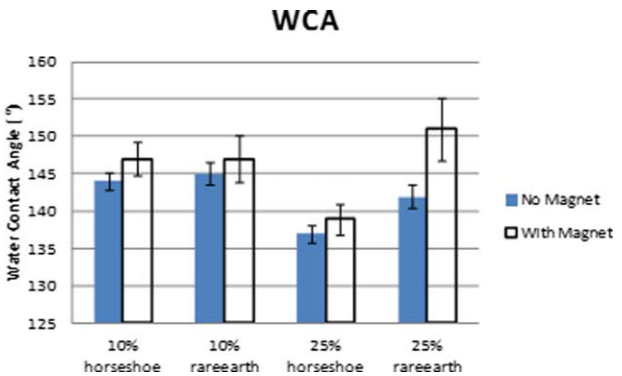

Figure 10. Magnetic particle embedded in polystyrene fiber—water contact angle. [Color figure can be viewed in the online issue, which is available at wileyonlinelibrary.com.]

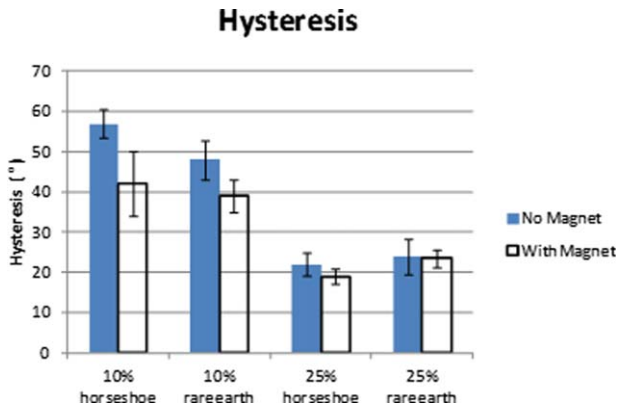

Figure 11. Magnetic particle embedded in polystyrene fiber—hysteresis. [Color figure can be viewed in the online issue, which is available at wileyonlinelibrary.com.]

increase in the surface roughness factor. That is, the magnetic field is physically moving the fibers and changing the surface morphology. The magnetic fabrics could, for example, be lifted off of a surface by the magnet. However, SEM imaging could not be performed in the presence of the magnet and attempts to visualize the field-induced morphology changes using optical microscopy were inconclusive due to insufficient resolution.

The results show conclusively that the hydrophobicity of electrospun PS/Fe magnetic fabrics can be adjusted through the application of an externally applied magnetic field. The externally applied field modifies both the contact angle as well as the contact angle hysteresis (stickiness) of the magnetic fabric. For the surfaces studied in this work, the applied magnetic field was found to increase the hydrophobicity and decrease the stickiness. Small, permanent magnets with limited strength were used in this study to qualitatively demonstrate the effect of magnetic field on the hydrophobicity of magnetic fabrics. We believe that, by optimizing the fabric properties and by using stronger electromagnets with tunable strength and field orientation it may be possible to develop smart fabrics with externally adjustable wettability.

CONCLUSIONS

Magnetic fabrics consisting of iron nanoparticles embedded within polystyrene fibers were produced using electrospinning. The magnetic fabrics were tested with and without an externally applied magnetic field. The results show that the magnetic field increases the hydrophobicity of the surface and decreases the contact angle hysteresis (a measure of the stickiness of the surface). The underlying mechanism responsible for the observed changes in hydrophobicity with magnetic field is most likely a field induced change in the surface morphology.

AUTHOR CONTRIBUTIONS

Thu N. Ho: Prepared solutions; performed electrospinning for fiber fabrication; performed contact angle and hysteresis measurement; analyzed and summarized data; drafted the article. Negar Ghochaghi: Performed material characterizations, especially SEM. Reviewed and approved the article. Gary Tepper, Research Adviser: Oversaw the research projects; held weekly meeting to discuss project's status and suggested ideas to move forward; revised and approved the article.

REFERENCES

1. Rothstein, J. O. *Annu. Rev. Fluid Mech.* **2010**, *42*, 89.
2. Jung, Y. C.; Bhushan, B. *Nanotechnology* **2006**, *17*, 4970.
3. Zhao, N.; Shi, F.; Wang, Z. Q.; Zhang, X. *Langmuir* **2005**, *21*, 4713.
4. Shi, F.; Wang, Z. Q.; Zhang, X. *Adv. Mater.* **2005**, *17*, 1005.
5. Shirtliffe, N. J.; Hale, G.; Newton, H. I.; Parry, C. C. *Langmuir* **2003**, *19*, 5626.
6. Erbil, H. Y.; Demirel, A. L.; Avci, Y.; Mert, O. *Science* **2003**, *299*, 1377.
7. Fresnais, J.; Chapel, J. P.; Poncin-Epaillard, F. *Surf. Coat. Technol.* **2006**, *200*, 5296.
8. Pozzato, A.; Zilio, S. D.; Fois, G.; Vendramin, D.; Mistura, G.; Belotti, M.; Chen, Y.; Natali, M. *Microelectron. Eng.* **2006**, *83*, 884.
9. Fredrick, O. O.; Samaha, M. A.; Tafreshi, H. V.; Tepper, G. C. *J. Appl. Polym. Sci.* **2012**, *123*, 1112.
10. Sarkar, S.; Deevi, S.; Tepper, G. *Macromol. Rapid Commun.* **2007**, *28*, 1034.
11. Jiang, L.; Zhao, Y.; Zhai, J. *Angew. Chem. Int. Ed.* **2004**, *43*, 4338.
12. Xue, Y.; Wang, H.; Yu, D.; Feng, L.; Dao, L.; Wang, X.; Lin, T. *Chem. Commun.* **2009**, 6418.
13. Ma, M.; Hill, R. M.; Lowery, J. L.; Fridrikh, S. V.; Rutledge, G. C. *Langmuir* **2005**, *21*, 5549.
14. Park, S. H.; Lee, S. M.; Lim, H. S.; Han, J. T.; Lee, D. R.; Shin, H. S.; Jeong, Y.; Kim, J.; Cho, J. H. *ACS Appl. Mater. Interfaces* **2010**, *2*, 658.
15. Uecker, J. C.; Tepper, G. C.; Rosell-Llompart, J. *Polymer* **2010**, *51*, 5221.
16. Fong, H.; Chun, I.; Reneker, D. H. *Polymer* **1999**, *40*, 4585.
17. Reneker, D. H.; Yarin, A. L. *Polymer* **2008**, *49*, 2387.
18. Tripatanasuwan, S.; Zhong, Z.; Reneker, D. H. *Polymer* **2007**, *48*, 5742.
19. Casie, A. B. D.; Baxter, S. *Trans. Faraday Soc.* **1944**, *40*, 546.
20. Hoefnagels, H. F.; Wu, D.; de With, G.; Ming, W. *Langmuir* **2007**, *23*, 13158.
21. Chao-Hua, X.; Shun-Tian, J.; Jing, Z.; Li-Qiang, T.; Hong-Zheng, C.; Mang, W. *Sci. Technol. Adv. Mater.* **2008**, *9*, 035008.
22. Berim, G. O.; Ruckenstein, E. *J. Chem. Phys.* **2008**, *129*, 114709.
23. Mateo, J. N.; Kulkarni, S. S.; Das, L.; Bandyopadhyay, S.; Tepper, G. C.; Wynne, K. J.; Bandyopadhyay, S. *Nanotechnology* **2011**, *22*, 035703.
24. Wang, M.; Singh H.; Hatton T. A.; Rutledge G. C. *Polymer* **2004**, *45*, 5505.
25. Gass J.; Poddar P.; Almand J.; Srinath S.; Srikanth H. *Adv. Funct. Mater.* **2006**, *16*, 71.
26. Sung Y. K.; Ahn B. W.; Kang T. J. *J. Magn. Magn. Mater.* **2012**, *324*, 916.